Chemical Vapor Deposition

DOI: 10.1002/cvde.200606472

Full Paper

Application of LTPL Investigation Methods to CVD-Grown SiC**

By *Jean Camassel*, *Sandrine Juillaguet*,* *Marin Zielinski*, and *Carole Balloud*

We review in detail the few (simple) theoretical equations that rule all near-equilibrium recombination processes in semiconductors with direct or indirect bandgaps. In the case of 4H-SiC, we discuss their physical significance and show the corresponding limits. Next, we discuss the effect of residual doping in 3C-SiC and show that, from typical low-temperature photoluminescence (LTPL) data, very simple estimates of the doping level can be made. Finally, we focus on aluminum doping in 4H-SiC. Performing a systematic comparison of LTPL spectra with secondary ion mass spectroscopy (SIMS) and/or capacitance-voltage measurements, we show that a reasonably good value of the residual (or intentional) doping level can be obtained from simple optical measurements. An interesting point is that, in many cases, the use of such optical techniques offers the non-negligible advantage to allow detection beyond the SIMS limit.

Keywords: 3C-SiC, 4H-SiC, Low-temperature photoluminescence, Nitrogen and aluminum doping, Secondary ion mass spectroscopy, Silicon carbide

1. Introduction

In modern semiconductor physics, LTPL spectroscopy is a well-established technique to perform fast, non-destructive but *qualitative* analyses of the residual doping *species* in as-grown, bulk, or epitaxial material.[1] In this way the *radiative* recombination signature of specific impurities in silicon, gallium arsenide, gallium nitride, and silicon carbide has been investigated in great detail for many years. In the case of SiC, such investigations have been made for residual or intentional donor species, either associated with nitrogen[2–5] and phosphorus,[6] or shallow acceptors like aluminum[7–9] and boron.[10] Unfortunately in many cases, a *comprehensive* and *quantitative* correlation between the change in LTPL intensity and the concentration of residual species is still lacking. Basically, what is done is that a normalized LTPL intensity curve is drawn for a given polytype versus SIMS concentration or (below the SIMS detection limit) versus results of capacitance-voltage (*C–V*) measurements obtained from a mercury probe or a similar technique. This curve is next used by the remaining part of the community as an untouchable standard but *no* physical discussion of the basic origin (and/or validity limit) of the concepts which support this calibration law is given. This is not only true for SiC,[2–5,8–9] but also (and exactly in the same way) for Si.[1,11]

In this work, we start from the standard equations that rule all near-equilibrium recombination processes in a semiconductor. In the case of 4H-SiC, we discuss their physical significance and show the corresponding limits. Next, we discuss the case of residual nitrogen doping in 3C-SiC and show that very similar estimates can be done. Finally, we discuss the case of aluminum doping in the 4H polytype. The paper is organized as follows. In Section 2, we review the theoretical background of LTPL spectroscopy. In Section 3, we consider the effect of residual n-type doping in 4H-, 6H-, and 3C-SiC, while in Section 4 we focus on the effect of p-type doping. We draw some conclusions in Section 5. Finally, in Section 6, we review some experimental details.

2. Theoretical Background

Basically LTPL is a very simple process, in which a high concentration of electron-hole pairs or free excitons (hereafter called FEs) is created by absorption of a flux of incoming photons. These FEs thermalize and, after some delay, re-

[*] Dr. S. Juillaguet, Dr. J. Camassel, Dr. C. Balloud
Groupe d'Etude des Semiconducteurs, Université Montpellier 2 and CNRS
cc 074-GES, 34095 Montpellier cedex 5 (France)
E-mail: sandrine.juillaguet@ges.univ-montp2.fr
Dr. M. Zielinski
CNRS-CRHEA
Rue Bernard Grégory, 06650 Valbonne (France)

[**] We greatly thank B. Boyer from University Montpellier 2 for expert assistance with the SIMS measurements. We also thank C. Sartel, V. Soulière, and Y. Monteil from Laboratoire des Multimatériaux et Interfaces in Lyon for providing numerous 4H-SiC samples. We thank D. Chaussende, M. Pons, and R. Madar from Institut National Polytechnique in Grenoble for the gift of the CF-PVT sample. Finally, we thank all members of the European Projects SOLSIC and FLASiC Consortia, specially Prof. Y. Stoemenos from Tessaloniki, G. Ferro from LMI (Lyon), T. Chassagne and A. Leycuras from CRHEA (Valbonne), L. Di Cioccio and P. Ferret from LETI/CEA (Grenoble) as well as A. Schöner from Acreo and A. Henry from Linköping University (Sweden) for continuous discussions and collaboration. We will not forget to thank the European Community for financial support through contracts SOLSIC (G5RD-CT-2001-00563) and FLASIC (G5RD- CT2002-00704).

combine (radiatively or non-radiatively). From a simple conservation law, often called the "detailed-balance principle",[12] the time-dependent concentration of free excitons, n_{FE} [cm^{-3}], obeys the basic rate equation, Equation 1.

$$\frac{dn_{FE}}{dt} = g_{FE} - \left(\frac{1}{\tau^{r}_{FE}} + \frac{1}{\tau^{nr}_{FE}}\right) n_{FE} - t_{RX} \quad (1)$$

In this expression, g_{FE} is the generation rate [cm^{-3} s^{-1}], while τ^{r}_{FE} and τ^{nr}_{FE} are the (intrinsic) radiative and non-radiative lifetimes (second) of the free electron-hole pairs, respectively. The transfer term t_{RX} [cm^{-3} s^{-1}] accounts for all possible (extrinsic) relaxation mechanisms toward one (or more) radiative (residual-impurity related) low energy state(s).

In high quality 4H-SiC and in the case of non-intentional doping, the residual level of impurities is low.[2,13] Moreover, in most cases it is believed that these impurities come only from the nitrogen species. At low temperature, they act as residual (neutral) donors which can bind a free exciton. In this case, t_{RX} reduces to t_{DX} (in which DX stands for an exciton bound to a neutral donor) and the corresponding concentration of bound electron-hole pairs, n_{DX}, obeys Equation 2, which is formally similar to Equation 1.

$$\frac{dn_{DX}}{dt} = t_{DX} - \left(\frac{1}{\tau^{r}_{DX}} + \frac{1}{\tau^{nr}_{DX}}\right) n_{DX} \quad (2)$$

In this case, τ^{r}_{DX} and τ^{nr}_{DX} are the radiative and non-radiative lifetimes of the donor bound excitons, while t_{DX} is the new (specific) generation term. Starting from two different entities (a neutral donor and a free exciton) it corresponds to the creation of a new (four particle) complex. In the first approximation, one can write the transfer term as Equation 3.

$$\tau_{DX} = n_{FE} f_{FE} [N]/[C] \quad (3)$$

n_{FE} is obtained from Equation 1, while f_{FE} is an average scattering frequency of FEs. The concentrations [N] and [C] refer to the concentration of nitrogen impurities and carbon sites that exist per cubic centimeter of material, respectively. The dimensionless ratio [N]/[C] is then the probability of a traveling (free) exciton to encounter (when scattering in the weakly doped SiC/N lattice) a neutral nitrogen atom sitting at a carbon site and, in this way, to transform into a new (DX) entity.

In this expression, the following point should be outlined. The ratio f_{FE}/[C] is nothing but a capture rate constant B_{FE} [cm^3 s^{-1}] similar to the one already introduced, many years ago, to describe the capture rate of a free electron in a solid. Following this path,[14] and given a mean velocity, $<V_{FE}>$, for the scattering FEs, B_{FE} can be written using Equation 4.

$$B_{FE} = <V_{FE}> \sigma_{FE} . \quad (4)$$

Strictly speaking, the cross section σ_{FE} [cm^2] refers to the direct capture rate of a free exciton (or electron-hole pair) by a neutral impurity. Of course, the real situation is not so simple and *no* free exciton is directly trapped, as a whole, by a single (neutral) atom. Instead of a given traveling pair, a neutral donor will bind first the traveling electron on a 2-electron (excited) state, while a neutral acceptor will bind the hole on a 2-hole excited state. The fourth partner will then come. A particular case is that of donor-acceptor pairs (DAPs) in which the two different partners are usually trapped (almost simultaneously) by two neighboring atoms (one ionized donor and one ionized acceptor). Taking into account all those considerations, one can write Equation 5.

$$\sigma_{FE} = \sigma_{E} + \sigma_{H} \quad (5)$$

Only σ_{E} (σ_{H}) has to be considered for a neutral donor (acceptor) bound exciton, while both participate in the case of an exciton bound to a (neutral) DAP.

Let us now come back to the main case of interest. We consider a standard DX complex under steady state conditions and write Equation 6.

$$\frac{dn_{FE}}{dt} = 0 \quad \text{and} \quad \frac{dn_{DX}}{dt} = 0 \quad (6)$$

The LTPL intensities coming from both radiative recombinations of FEs (I_{FE}) and DX bound excitons (I_{DX}) are given by Equation 7.

$$I_{FE} = \frac{n_{FE}}{\tau^{r}_{FE}} \quad \text{and} \quad I_{DX} = \frac{n_{DX}}{\tau^{r}_{DX}} \quad (7)$$

Solving Equations 1 and 2 versus N_D, we get for the lines intensities the picture shown in Figure 1. At low impurity concentration, only I_{FE} shows an intensity which depends

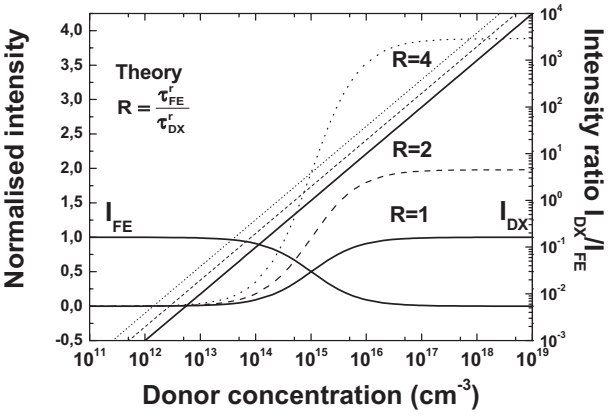

Fig. 1. Schematic drawing of the radiative recombination intensities expected for a free exciton (I_{FE}) and a donor bound exciton (I_{DX}) versus donor concentration. Notice the change by a factor of 4 (on the left scale) of the I_{DX} intensity when the radiative lifetime of the donor bound excitons decreases by a factor of 4. Also shown is the dimensionless ratio (I_{DX}/I_{FE}) versus donor concentration. Notice the linear dependence and the simple upward shift, when the radiative lifetime of donor bound excitons decreases.

only on the intrinsic material parameters. By increasing N_D above a certain threshold value (10^{13} to 10^{14} cm^{-3} in this case), I_{DX} starts to show and increases progressively while I_{FE} decreases. On increasing N_D further, the transfer becomes complete and, provided both exciton features have similar decay times, I_{DX} finishes with an intensity similar to I_{FE}. Of course, when the time characteristics differ, the asymptotic values differ. This is illustrated for typical values of the ratio τ^r_{FE}/τ^r_{DX}equal to 1, 2, and 4. The shorter the radiative lifetime of the bound exciton complex, the higher is the line intensity.

A more interesting result appears when, instead of the separated lines intensities, the direct (dimensionless) ratio I_{DX}/I_{FE} is considered. From Equation 1 and 2, we form Equation 8.

$$\frac{I_{DX}}{I_{FE}} = \frac{\tau^r_{FE}\tau^{nr}_{DX}}{\tau^r_{DX}} f_{FE}[N]/[C] = K[N] \quad (8)$$

This simple expression, which does not depend on a large number of materials parameters, on experimental values of the incident pumping power, or on critical details of the band structure of the material under consideration, is illustrated (again for three different values of the ratio τ^r_{FE}/τ^r_{DX}) as straight lines in Figure 1. The dimensionless parameter, A, is defined in Equation 9.

$$A = \frac{\tau^r_{FE}\tau^{nr}_{DX}}{\tau^r_{DX}} f_{FE} \quad (9)$$

This shows that one can directly estimate (in any low-doped material) the concentration of residual impurities, R, sitting at a lattice site, S, from the ratio of integrated intensities of the relative excitonic lines, as shown in Equation 10.

$$[R] = A^{-1}[S]I_{RX}/I_{FE} \quad (10)$$

This is a well-known result for silicon,[1] in which both the concentration of residual donors (phosphorus) and acceptors (aluminum and boron) have been probed in this way.[11] This has also been found for the residual nitrogen species in 4H and 6H-SiC.[3] However, in this case with respect to elemental Si, the experimental situation is more complicated.

Consider, for instance, 4H-SiC. Firstly, because of the large unit cell, there are 24 optically active phonon modes (instead of 4 in Si), which couple in different ways with all (free or bound) zero-phonon wave-functions. This results in 24 (different) phonon replicas per zero phonon line (ZPL) with 24 different intensities.[14] Secondly, there are (at least) two ZPLs associated with the radiative recombination of FEs bound to a given series of neutral donor (or acceptor) species. For nitrogen in 4H-SiC, they have been called P_0 and Q_0, and refer to the hexagonal and cubic lattice sites, respectively. For a more detailed description, see the literature[2–5,13] and references therein. Altogether, this results in basically ~1250 possible (independent) combinations of I_{DX} - E_{phonon}/I_{FE} - E_{phonon} lines. Of course, only the ones corresponding to the most intense components are usually considered.

3. Application to n-Type Doped SiC

As indicated, Equation 8 works extremely well in the case of hexagonal SiC. This is shown in Figure 2, and was clearly demonstrated in the work of Ivanov et al.[3] Considering a series of 4H- and 6H-SiC samples grown in a hot-wall CVD reactor, Ivanov et al. demonstrated that the ratio $I_{Q0}/I_{FE\text{-}77}$ scales linearly (on a log-log scale) versus nitrogen concentration. This was established from the low residual

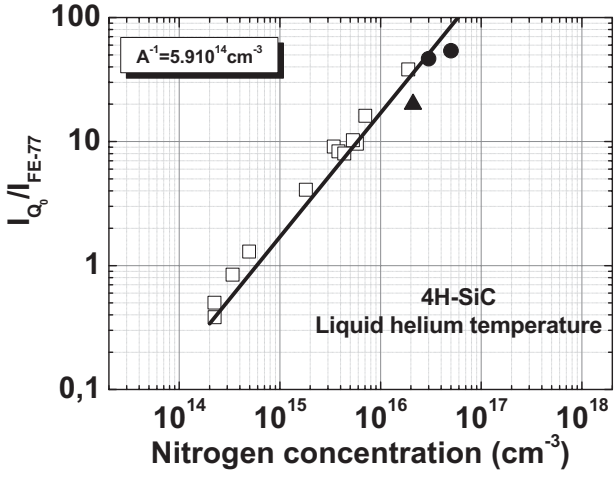

Fig. 2. Experimental values of the intensity ratio $I_{Q0}/I_{FE\text{-}77}$ in 4H-SiC plotted versus nitrogen concentration. The open squares are experimental data obtained from the literature [3]. Also shown as full symbols are experimental results obtained in this work using *C–V* (dots) and SIMS (triangle) measurements to determine the residual donor concentration. The solid line is a least mean square fit according to Eq. 8. The value of the final slope (5.9×10^{14} cm^{-3}) is very close to the that (5.2×10^{14} cm^{-3}) found in the literature [3].

impurity content (~2×10^{14} cm^{-3} in both polytypes) up to a final value, which depended slightly on the polytype under investigation (~2×10^{16} N cm^{-3} in 4H and 1×10^{17} N cm^{-3} in 6H). From these results, they obtained slope parameters, $K^{-1} = 5.2 \times 10^{14}$ cm^{-3} for 4H and $K^{-1} = 1.1 \times 10^{15}$ cm^{-3} for 6H.

Using for [C] the value 9.65×10^{22} cm^{-3} obtained from standard structural parameters, this gives, for the ratio of lifetimes and collision frequencies entering Equation 9, $A = 1.85 \times 10^8$ for 4H and $A = 0.88 \times 10^8$ for 6H.

Taking in both cases $\tau^{nr}_{FE} = \tau^{nr}_{DX} = 10$ ns,[15] and assuming that the radiative lifetime of free excitons (τ^r_{FE}) remains in a similar range (10 to 100 ns), the scattering frequency f_{FE} has a range of 10^{15} to 10^{16} collisions per second. This is much higher than the collision frequency estimated from

transport experiments for electrons and holes at the band edge (even in high quality material[16]) and suggests that the thermal decay from FE states to the DX ones is a "hot-exciton" process, which happens in the first few femtoseconds after excitation. Of course, the same approach should be valid for aluminum or phosphorus. Unfortunately, *no* similar result has been reported up to now for these doping species. With respect to silicon,[11] this shows that (even considering the most advanced 4H polytype) the growth technology of SiC is still in its infancy.

To complement these results, we have tried to extend the work of Ivanov et al.[3] from a concentration of 2×10^{16} in 4H to ~1×10^{17} cm^{-3} (full symbols in Fig. 2). This turned out to be extremely difficult. When the donor concentration increases, even the most intense phonon replica of the FE line disappears rapidly, and we could go no higher than 5×10^{16} cm^{-3}. To go a step further, one has to consider additional features such as, for instance, intra bound-exciton complex exchanges of which a typical example is shown in Figure 3. At low doping levels (5×10^{16} cm^{-3}) we notice that both the 77 meV phonon replica of the intrinsic ZPL (I_{77}) or the P_0 line, and the 77 meV phonon replica (P_{77}) or the

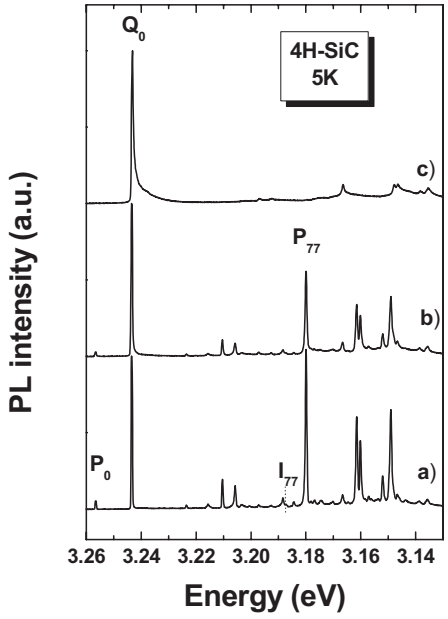

Fig. 3. Example of LTPL spectra collected at 5K on three different samples of 4H-SiC, with nitrogen donor concentration ranging from 5×10^{16} cm^{-3} (sample a) to 2.4×10^{17} cm^{-3} (sample b) and 1.2×10^{18} cm^{-3} (sample c). All donor concentration values were extracted from *C–V* measurements. Notice the rapid disappearance of the FE component (annotated I_{77}) and the progressive change in intensity of the ratio Q_0/P_{77} when the nitrogen concentration increases.

Q_0 line still resolve simultaneously. This makes the use of the previous technique difficult, but still possible. For illustration, the corresponding data points have been shown as full symbols in Figure 2. However, increasing the doping level again, I_{77} disappears, P_{77} decreases, and Q_0 becomes the most important line. When continuing to increase the doping level, the interesting point is that the ratio Q_0/P_{77} continues to vary. If we remember that Q stands for the cubic sites and P for the hexagonal sites, what happens is clearly a competition between the thermalization of FEs at the cubic and hexagonal sites versus donor concentration. This was first recognized by Henry et al.[5] for 4H-SiC, with experimental data shown as open triangles in Figure 4. We find the same qualitative trend (full symbols) but a detailed description is out of the scope of this work. We simply notice that this is *not* specific for 4H-SiC. The same behavior

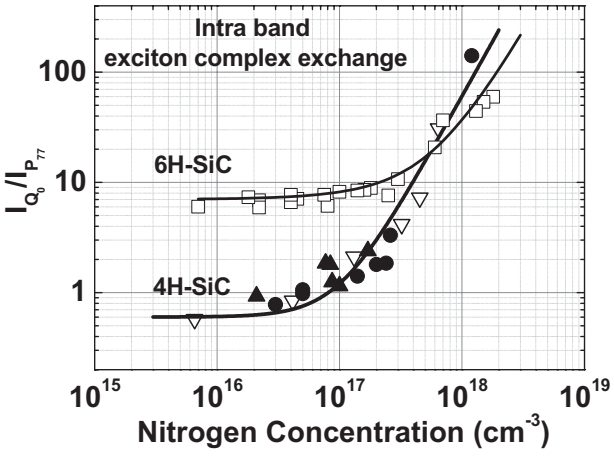

Fig. 4. Examples of intra-bound exciton complex exchanges (i.e., concentration dependence of the ratio of bound exciton lines) observed in the case of 6H-SiC (upper curve) and 4H-SiC (lower curve). In both cases, a guide to the eye is given. Each was fitted using Eq. 11 using the parameter values listed in Table 1. Full symbols are experimental data obtained in this work for 4H-SiC. *C–V* (dots) and SIMS (triangle) measurements were used to deduce the residual donor concentration. Open inverse triangles are from previous work [5]. Open squares are taken from the literature [17].

should be found in any SiC polytype with a large rhombohedral or hexagonal unit cell, and was indeed (independently) identified by Weingärtner and co-workers[17] for 6H-SiC. The corresponding data are shown as open squares in Figure 4. Notice that the solid lines are guides to the eye in both cases. They have been computed according Equation 11.

$$(I_{DX})_C/(I_{DX})_H = R_0 + R_1 N_d + R_2 N_d^2 \quad (11)$$

R_0, R_1, and R_2 have values listed in Table 1 for 4H- and 6H-SiC. It is important to note that the same behavior *cannot* be found in Si, GaP, or even 2H- and 3C-SiC. This is because there is only one site symmetry (cubic or hexagonal) allowed for substituted atoms in such high symmetry crystals.

Increasing the doping level again, there is no longer any P_{77} line to compare with and (at very high doping levels) the only sensitive parameters remain the broadening and shift of the Q_0 line. This was first recognized by Forsberg et al.,[4] and comes from the change in scattering frequency of

Table 1. List of parameters used in Eq. 11 to draw the lines used as guides to the eye shown in Fig. 4.

Polytype	R_0	R_1 [cm^3]	R_2 [cm^6]
6H-SiC	6.5	1×10^{-17}	2×10^{-35}
4H-SiC	0.7	3×10^{-18}	5×10^{-35}

excitons when the donor concentration increases. In Figure 5, we show that the same behavior is found in the case of 3C-SiC. We consider various samples (from different origins) grown in various set-ups using different techniques. First, we notice that (whatever the sample origin) one always finds five lines (labeled ZPL, TA, LA, TO, and LO)

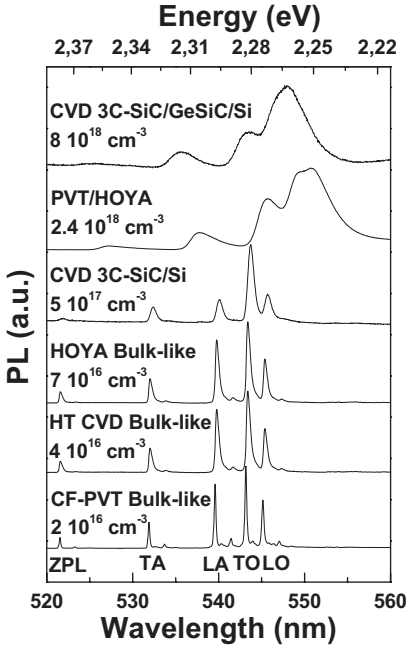

Fig. 5. Examples of LTPL spectra collected at 5K on various 3C-SiC samples with different nitrogen concentrations. The sample origin and nitrogen concentration obtained from *C–V*, Hall, or SIMS measurements are listed in Table 2.

which are all (again) donor-bound exciton features. However, in 3C-SiC, there is usually *no* FE (radiative) recombination component to compare with. Referring to Figure 1, this means that we are dealing with a semiconductor system in which R is always very large. There is also no site competition to compare intensities from one site to the other one. This is because all substitutional sites are cubic. One is then left with one possibility, considering the change in broadening of the DX-exciton lines. Hopefully, this is a very sensitive method. Moving the doping level from a low 10^{16} to a high 10^{18} cm^{-3}, the PL line width changes by more than one order of magnitude.

Since we want to establish a calibration curve, a prerequisite is to avoid any possible artifact when comparing the line width and the doping level. In this work, we have used three different techniques (SIMS, Hall effect, and Raman measurements) to measure the concentration of free carriers (or doping species). For more details, see Section 6. The results are listed in Table 2. Concentrating on the broadening of the TA-phonon line, we plotted then in Figure 6 (on a log-log scale) the FWMH versus doping level. We find a good straight line, given by Equation 12.

$$[\Gamma_{TA}]_{3C} = A_{3C}[N]^{1/n} \tag{12}$$

Using $A_{3C} = -6.435$ and $n = 2.518$, we find that this equation works extremely well in the concentration range 10^{15} cm^{-3} to 10^{19} cm^{-3} and, to explain these results, one has to make a hypothesis.

We assume that increasing the doping level does not introduce any (new) impurity state at low energy. In other words τ_{DX}^{nr} in Equation 2 remains constant and the population of bound excitons increases regularly versus donor

Table 2. Nitrogen doping concentration determined by a) *C–V*, b) Hall effect, c) SIMS, d) micro-Raman investigations, and e) extrapolated. The samples investigated come from different origins.

Sample	N_D [cm^{-3}]	Reference
CVD Acreo on HAST	3×10^{15} [a]	18
CF-PVT bulk	6.5×10^{15} [e]	19
CVD on CF-PVT	3×10^{16} [a]	20
HT-CVD Free standing	4.2×10^{16} [d]	21
HAST (bulk like)	7×10^{16} [d]	22
CVD 3C-SiC/Si	4×10^{17} [b]	23
CVD 3C-SiC/Si	5×10^{17} [b]	23
CVD 3C-SiC/Si	1.4×10^{18} [c]	23
CVD 3C-SiC/Si	1.5×10^{18} [c]	23
Sublimation (on HAST)	5×10^{18} [d]	24
CVD 3C-SiC/GeSiC/Si	8×10^{18} [c]	25

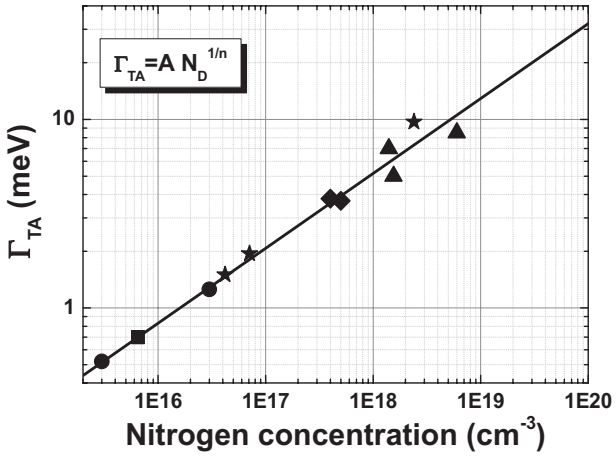

Fig. 6. Log-log plot of the broadening of the TA-phonon line in 3C-SiC versus nitrogen concentration. The experimental data are shown as full symbols. The broadening of the near band-edge TA-phonon line was obtained from experimental LTPL spectra, focusing on the replicas of the ZPL line. The nitrogen concentrations were determined by *C–V* (circles), SIMS (triangles), Hall (diamonds), and Raman (stars) measurements, respectively. The solid line corresponds to the theoretical fit. The samples origin and nitrogen concentration are listed in Table 2.

concentration. Then, after a critical value is reached, a new scattering process occurs, which increases the recombination rate. In other words, starting from a certain (unknown) critical concentration, the radiative lifetime decreases. Assuming that the sensitive parameter is the ratio of the Bohr radius of bound excitons to the nearest impurity-impurity distance (inverse cubic root of the concentration) one can write Equation 13.

$$\tau^{r}_{DX} = \left[\tau^{r}_{DX}\right]_0 \left(1 + \frac{r_{DX}}{r_{N-N}}\right) \tag{13}$$

As the concentration increases, the scattering rate increases and the radiative lifetime decreases as the inverse third power of the concentration. The integrated intensity changes then from a narrow delta-like function to a much broader line. In a first approximation, this can be modeled as Equation 14.

$$I_{PL} = I_N \delta[(\Omega - \Omega_0), \Gamma_N] = \int I_N \Gamma_N / \left[(\Omega - \Omega_0)^2 + (\Gamma_N)^2\right] d\Omega \tag{14}$$

This expression shows that both the line-width and the maximum intensity should depend on the concentration. Since a comparison of the line intensities is always difficult, to further check this idea we have focused on the line-width. From the results shown in Figure 6, we find a very reasonable linear rate with slope parameter 2.52 instead of 3. Taking into account all simplifying assumptions, this is rather satisfactory.

4. Aluminum Doping

In many SiC samples, unless intentionally doped, aluminum is *not* the most important residual impurity. It appears only like a new trapping center, which basically competes with nitrogen to bind a free exciton. This is exemplified in Figure 7. We show three near band edge LTPL spectra collected on three unintentionally doped 4H-SiC samples. In all three cases Al is present but, because the doping level is low, no donor acceptor pair (DAP) transition is seen. Simply between the well identified P_0 and Q_0 ZPLs, a new series of bound exciton lines appear, labeled $4Al_0$ by Clemen et al.[7] The interesting point is that the LTPL signal is dominated either by the DX (N-bound) or the AX (Al-bound) recombination lines, depending on the Al concentration determined by SIMS.

From the theoretical point of view (see Sec. 2) this means that we have to solve a set of three coupled equations. Since we notice at the same time the presence of two residual impurities, namely one donor (nitrogen) and one acceptor (aluminum), and since both compete to bind the same population of free excitons, we follow the path given by Schmidt et al.[26] We write the total transfer terms, t_{RX} in

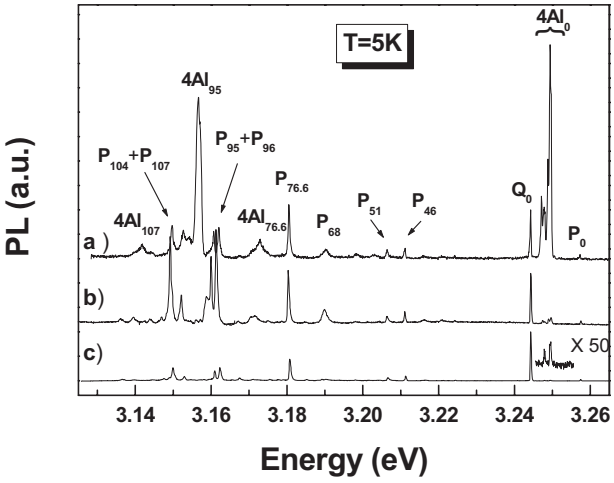

Fig. 7. LTPL spectra collected on 4H-SiC samples with aluminum concentrations a) 2.5×10^{16} cm^{-3}, and b) 4.7×10^{14} cm^{-3}. The concentrations for a) and b) were determined by SIMS. The concentration for c) was below the SIMS detection limit.

Equation 1, as the sum of the two independent contributions t_{DX} and t_{AX}, in which DX and AX stand for the excitons bound to a neutral donor or a neutral acceptor atom. Then Equation 1 becomes Equation 15.

$$\frac{dn_{FE}}{dt} = g_{FE} - \left(\frac{1}{\tau^{r}_{FE}} + \frac{1}{\tau^{nr}_{FE}}\right) n_{FE} - t_{DX} - t_{AX} \tag{15}$$

Equation 2 becomes Equation 16.

$$\frac{dn_{DX}}{dt} = t_{DX} - \left(\frac{1}{\tau^{r}_{DX}} + \frac{1}{\tau^{nr}_{DX}}\right) n_{DX} - t^{DX}_{AX} \tag{16}$$

Of course, this should be complemented by a third equation, Equation 17.

$$\frac{dn_{AX}}{dt} = t_{AX} + t^{DX}_{AX} - \left(\frac{1}{\tau^{r}_{DX}} + \frac{1}{\tau^{nr}_{DX}}\right) n_{AX} \tag{17}$$

In these expressions, τ^{r}_{AX} and τ^{nr}_{AX} stand (as usual) for the radiative and non-radiative lifetimes of the acceptor bound excitons, while the new transfer terms t_{AX} and t^{DX}_{AX} can be written as Equations 18 and 19.

$$t_{AX} = n_{FE} f_{FE} [Al]/[Si] \tag{18}$$

$$t^{DX}_{AX} = n_{DX} f_{DX} [Al]/[Si] \tag{19}$$

As in Section 2, the PL intensity of the different lines can be written as Equation 20.

$$I_{FE} = \frac{n_{FE}}{\tau^{r}_{FE}}, \quad I_{DX} = \frac{n_{DX}}{\tau^{r}_{DX}}, \quad \text{and} \quad I_{AX} = \frac{n_{AX}}{\tau^{r}_{AX}} \tag{20}$$

Strictly speaking, since the equations are not independent, they should be solved self-consistently. However,

since we focus on the simple case in which I_{FE} equals zero (see Fig. 7), we can work in a simplified model. We assume that there are no free excitons (no Eq. 15) but only donor-bound excitons (with concentration n_{DX}) which thermalize to the bound acceptor states. In this way, after some straightforward manipulations, we get Equation 21.

$$\frac{I_{AX}}{I_{DX}} = \frac{\tau^{r}_{DX}\tau^{nr}_{AX}}{\tau^{nr}_{DX}\tau^{r}_{AX}}\frac{[Al]}{[N]} \qquad (21)$$

This expression, which is formally similar to Equation 8, shows that in most semiconductor materials (and not only in SiC) the ratio of recombination line intensities I_{AX}/I_{DX} associated with the two main exciton complexes (AX and DX) should be a linear function of the concentration ratio [A]/[D].

To check this point further, we fitted the $4Al_0$ line intensity in different samples with a Gaussian profile. Then we normalized these intensities by computing the ratio $R = 4Al_0/Q_0$ (in which again Q_0 stands for the integrated intensity). Finally, we plotted the results in Figure 8 (again on a log-log scale) versus Al concentration obtained from independent SIMS measurements. The reasonable linear behavior shows that all Al atoms detected by SIMS act as electrically active impurities. Indeed, if that is true, one would expect for log(R) vs. log[Al] a slope equal to unity. From the experimental slope value, we conclude that (at least in this concentration range ~10^{15} to 10^{17} cm^{-3}) all Al atoms act as substitutional acceptors.

Because we normalize all data to the intensity of the Q_0 line, a key point is that the residual nitrogen concentration should *not* vary from sample to sample. This has been checked for the series of samples considered in this work, and we have only used samples with residual N concentration close to 1.5×10^{17} cm^{-3}. Of course, changing the residual N concentration (i.e., changing the growth conditions or growth facility) should not change the slope parameter, but should simply shift the solid line. This is exemplified in Figure 8 (broken lines) for residual nitrogen concentrations of 1.5×10^{15} and 1.5×10^{18} cm^{-3}.

A last point we want to emphasize is that, when the $4Al_0$ LTPL signature is weak, one can reach compensation values which are well below the SIMS detection limit. Typical examples are shown as star symbols in Figure 8.

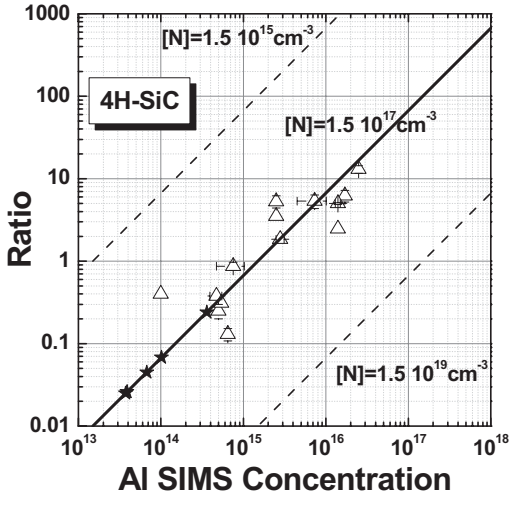

Fig. 8. Log-log plot of the integrated ratio calculated from experimental LTPL data versus aluminum concentration determined by SIMS. The open triangles represent experimental values of the ratio $R_0 = Al_0/Q_0$. They were used to compute the solid line, which corresponds to an average nitrogen concentration level of ~1.5×10^{17} cm^{-3}. The broken lines have been shifted assuming a lower and higher nitrogen compensation level, respectively. Typical values are 1.5×10^{15} cm^{-3} and 1.5×10^{19} cm^{-3} for the upper and lower line, respectively. The stars are extrapolated values, below the SIMS detection limit.

5. Conclusions

Starting from a simple correlation between LTPL data and SIMS (or *C-V*) measurements we have shown that it should be possible to perform simple, non-destructive, optical examinations of the residual impurity content in many semiconductor systems. The interesting point with such non-destructive (all-optical) techniques is that they can easily go beyond the usual SIMS detection limit, or to investigate samples with a low level of residual impurities, on which (for some reason) *C-V* measurements are difficult to make. In SiC, this covers the range of nitrogen concentration from 10^{14} cm^{-3} to 10^{19} cm^{-3}, and aluminum concentration from 10^{13} cm^{-3} (below the usual SIMS detection limit) up to ~2×10^{18} cm^{-3}.

6. Experimental

Samples: Unless specifically indicated, most of the experimental results considered for n-type 4H- and 6H-SiC have been extracted from the tutorial works in the literature [3–5]. When necessary, additional results have been obtained from samples grown at Laboratoire des Multimatériaux et Interfaces (LMI) in Lyon (France). The growth set-up was a vertical, cold-wall reactor a described previously [27]. The residual nitrogen level was approximately 10^{16} cm^{-3} and, when necessary, aluminum doping was made [28] using trimethyl aluminum (TMA) provided by Epichem [29]. Concerning the 3C-SiC samples, they were of much different origins. For additional details, see Section 3.

Collecting LTPL Spectra: Because of the indirect bandgap structure of SiC which results in a relatively poor luminescence efficiency (typically 1/1000° of the one of GaN), one needs always a high excitation density combined with a short excitation wavelength to collect significant LTPL signals from a thin epitaxial layer. All experimental spectra considered in this work have been collected at 5K, using about 20 mW of the 244 nm wavelength of a frequency doubled (FreD) argon-ion laser as excitation source. A Triax 550 spectrometer from Jobin Yvon, fitted with 2400, 1200, and 600 gr mm^{-1} gratings and a cooled UV-CCD camera, completed the set up. The typical acquisition time was about one minute per spectrum.

C-V, *Hall*, *Raman and SIMS Measurements*: All *C–V* measurements were made using a mercury probe. In some cases, Hall measurements were done. In this case, we used the experimental procedure and analyses techniques described in the literature [16]. In some other cases, the free carrier concentration was deduced from Raman measurements using the extraction procedure described in the literature [30,31]. For the SIMS analyses, we used a IMS 5f mass spectrometer from Cameca. To analyze the nitrogen concentration, we used a 10 keV $^{133}Cs^{+}$ source. The negative (–4.5 keV) $^{13}C^{14}N^{-}$ secondary ions were detected using a mass resolution (dM/M~1/5000) to minimize the interference effect of $^{13}C^{14}N^{-}$ ions with other $^{27}X^{-}$ species. Using

a primary current of ~100 nA and a crater size of 150 μm × 150 μm, a typical erosion rate of ~1 nm s^{-1} was achieved. The $^{13}C^{14}N^-$ ions were collected from a 30 μm diameter spot in the central part of the craters. For aluminum, the depth profiles were measured using a 15 keV $^{16}O_2^+$ source, and detecting the positive (+4.5 keV) secondary ions. The primary current (~600 nA) and the crater size (150 μm × 150 μm) resulted in a sputtering rate of ~3 nm s^{-1}. Similar to nitrogen, the $^{27}Al^+$ ions were collected from a 30 μm diameter spot in the central part of the crater. The detection limit (DL) was 2×10^{16} cm^{-3} to 1×10^{17} cm^{-3} for nitrogen, depending slightly on the vacuum conditions. This is to be compared with 1×10^{14} cm^{-3} for Al. Running through the entire series of p-type doped samples, the Al concentration (as determined by SIMS) varied from 1×10^{14} to 1×10^{18} cm^{-3} In some cases, an extra Al contamination of the near-surface region (up to ~200 nm) was observed. Such a contribution, which presents some inhomogeneity across the sample surface, should not influence significantly the PL spectra. It was not taken into account in the estimation of the average sample concentration.

Received: March 15, 2006
Final version: May 16, 2006

[1] For a recent review see, S. Perkowitz, *Optical Characterisation of Semiconductors*, Academic Press, London **1994**.
[2] a) W. J. Choyke, D. R. Hamilton, L. Patrick, *Phys. Rev.* **1964**, *133*, A-1163. b) L. Patrick, W. J. Choyke, D. R. Hamilton, *Phys. Rev.* **1965**, *137*, A-1515.
[3] a) I. G. Ivanov, C. Hallin, A. Henry, O. Kordina, E. Janzen, *J. Appl. Phys.* **1996**, *80*, 3504. b) A. Henry, O. Kordina, C. Hallin, C. Hemmingsson, E. Janzen, *Appl. Phys. Lett.* **1994**, *65*, 2457.
[4] U. Forsberg, A. Henry, M. K. Linnarsson, E. Janzen, *Mater. Sci. Forum* **2000**, *338–342*, 619.
[5] A. Henry, A. Ellison, U. Forsberg, B. Magnussin, G. Pozina, E. Janzen, *Mater. Sci. Forum* **2002**, *389–393*, 593.
[6] S. G. Sridhara, L. L. Clemen, D. Nizhner, R. P. Devaty, W. J. Choyke, D. J. Larkin. *Mater. Sci. Forum* **1998**, *264–268*, 465.
[7] L. L. Clemen, R. P. Devaty, M. F. MacMillan, M. Yoganathan, W. J. Choyke, D. J. Larkin, J. A. Powel, J. A. Edmond, H. S. Kong, *App. Phys. Lett.* **1993**, *62*, 2953.
[8] S. Juillaguet, M. Zielinski, C. Balloud, C. Sartel, C. Consejo, B. Boyer, V. Soulière, J. Camassel, Y. Monteil, *Mater. Sci. Forum* **2004**, *457–460*, 775.
[9] M. Zielinski, C. Balloud, S. Juillaguet, B. Boyer, V. Soulière, J. Camassel, *Mater. Sci. Forum* **2005**, *483–485*, 449.
[10] S. G. Sridhara, L. L. Clemen, R. P. Devaty, W. J. Choyke, D. J. Larkin, H. S. Kong, T. Troffer, G. Pensl, *J. Appl. Phys.* **1998**, *83*, 7909.
[11] P. McL. Colley, E. C. Lightowlers, *Semicond. Sci. Technol.* **1987**, *2*, 157.
[12] J. I. Pankove, *Optical Processes in Semiconductors*, Dover Publications, Mineola, NY **1975**.
[13] a) I. G Ivanov, U. Lindelfelt, A. Henry, O. Kordina, C. Callin, M. Aroyo, T. Egilsson, E. Janzen, *Phys. Rev.* **1998**, *B58*, 13 634. b) R. P. Devaty, W. J. Choyke, *Phys. Status Solidi A* **1997**, *162*, 5.
[14] M. Lax, *Phys. Rev.* **1960**, *119*, 1502.
[15] J. P. Bergman, O. Kordina, E. Janzen, *Phys. Status Solidi A* **1997**, *162*, 65.
[16] J. Pernot, S. Contreras, J. Camassel, *J. Appl. Phys.* **2005**, *98*, 23 706.
[17] R. Weingärtner, A. Albrecht, P. J. Wellmann, A. Winnacker. *Mater. Sci. Forum* **2003**, *433–436*, 341.
[18] A. Schöner, *Final SOLSiC report*, (GSRD-CT-2001-00563).
[19] D. Chaussende, L. Latu Romain, L. Auvray, M. Ucar, M. Pons, R. Madar, *Mater. Sci. Forum* 2005, *483–485*, 225.
[20] P. Ferret, LETI-CEA, private communication.
[21] G. Ferro, C. Balloud, S; Juillaguet, P. Vicente, J. Camassel, Y. Monteil, *Mater. Sci. Forum* 2003, *433–436*, 115.
[22] www.hast.jp
[23] G. Ferro, J. Camassel, S. Juillaguet, C. Balloud, E. K. Polychroniadis, Y. Stoemenos, J. Dazord, H. Peyre, Y. Monteil, S. A. Rushworth, L. M. Smith, *Semicond. Sci. Technol*. 2003, *18*, 1.
[24] E. Polychroniadis, M. Syvajarvi, R. Yakimova, J. Stoemenos, *J. Cryst. Growth* 2004, *263*, 68.
[25] J. Pezoldt, *Final FLASiC report*, (GSRD-CT-2002-00704).
[26] T. Schmidt, K. Lischka, W. Zulehner, *Phys. Rev.* **1992**, *B45*, 8989.
[27] C. Sartel, C. Balloud, V. Soulière, S. Juillaguet, J. Dazord, Y. Monteil, J. Camassel, S. Rushworth, *Mater. Sci. Forum* **2004**, *457–460*, 217.
[28] C. Sartel, V. Soulière, M. Zielinski, Y. Monteil, J. Camassel, S. Rushworth, *Mater. Sci. Forum* **2005**, *483–485*, 121.
[29] www.epichem.co.uk
[30] S. Nakashima, H. Harima, *Phys. Status Solidi A* **1997**, *162*, 39.
[31] J. Camassel, P. Vicente, L. A. Falkovski, *Mater. Sci. Forum* **2001**, *353–356*, 335.

